A Further Study on Calcium Phosphate Gardens Grown from the Interface of κ-Carrageenan-based Hydrogels and Counterion Solutions

Fogde, Anna; Rosqvist, Emil; Le, Trung-Anh; Smått, Jan-Henrik; Sandberg, Thomas; Huynh, Tan-Phat

Published in:
ChemPlusChem

DOI:
10.1002/cplu.202200426

Published: 01/02/2023

Document Version
Accepted author manuscript

A Further Study on Calcium Phosphate Gardens Grown from the Interface of κ-Carrageenan-based Hydrogels and Counterion Solutions

*Anna Fogde[1,2], Dr. Emil Rosqvist[1], Trung-Anh Le[1], Dr. Jan-Henrik Smått[1], Dr. Thomas Sandberg[1], Dr. Tan-Phat Huynh[1,]**

[1] Laboratory of Molecular Science and Engineering, Åbo Akademi University, FI-20500, Turku, Finland

[2] Department of Mechanical and Materials Engineering, University of Turku, FI-20014 Turku, Finland

ABSTRACT Originating from the concept of classical chemical gardens, a new field coined 'chemobrionics' has recently emerged. In the present work, two chemobrionic systems grown

from a hydrogel/liquid interface at different time scales (for 1, 7, 14 or 28 days) were investigated, i.e., a calcium-based hydrogel with a phosphate counterion solution (Ca-gel) and a phosphate-based hydrogel with a calcium counterion solution (P-gel). The initial pH changes of the systems were investigated, and the obtained tubular structures were studied using optical microscopy, SEM, AFM, PXRD and TGA. One of the important findings is the tubes obtained in the Ca-gel system were straight and longer, which could be explained by the larger pH difference observed between the hydrogel and the counterion solution in this system (ΔpH ~2.1) compared to the P-gel system (ΔpH ~0). The Ca-gel structures remained overall more amorphous even though increased crystallinity was observed in both systems with increased time spent in counterion solution. Both systems contained hydroxyapatite phases, with additional calcite phases observed for the P-gel structures and traces of κ-carrageenan for the Ca-gel structures. Our study provides a promising method for making tubular macrostructures through controlling the reaction conditions such as maturation time and pH.

INTRODUCTION

Classical chemical gardens that are grown by placing a seed of a soluble metal salt into anionic solutions such as silicates, carbonates or phosphates, are well-known.[1–3] Especially gardens grown in silicate solution are popular in the chemistry classroom as demonstrations or laboratory experiments and can even be found as part of chemistry kits intended for home use.[1,4,5] Formation of chemical gardens involves a precipitation reaction giving rise to a semipermeable membrane. The state of the solution inside of the membrane differs from that on the outside, with a steep gradient of concentration and pH, causing an osmotic flow, continuously dissolving the metal salt seed within the membrane. This process will continue stretching the membrane until it ruptures. As this happens, a jet of fluid is ejected into the surrounding solution, giving rise to a new membrane over which the process of osmotic flow

will continue. Thus, the process of rupturing and creation of new membranes continues in cycles.[2,6] With the self-organizing structures of the chemical gardens as a starting point, a new and wider field that has been termed 'chemobrionics' has emerged, intersecting chemistry, materials science, biology and physics. The broad field of the chemobrionic research on nano- and microtubular structures bestow new understanding of subjects such as nonlinear and complex systems as well as understanding of the origin of life.[6,7] It has also given rise to new methods and materials in fields such as sensing[8,9] and biomedical engineering, for example in the form of calcium phosphates.[10,11] The kind of chemobrionic tubular structures found in the classical chemical gardens can also be grown using a hydrogel loaded with ions as the seed.[12–14] Hydrogels used for this purpose have for example been based on agar[13,15] and gelatin[12]. In our previous work, we have shown that it is also possible to grow two different types of calcium phosphate gardens from an interface between a κ-carrageenan hydrogel and a counterion solution.[14]

Carrageenans are a family of polysaccharides, hydrophilic and linear sulfated galactans, that can be extracted from the *Rhodophyta* species of red seaweeds.[16–18] The carrageenan structure mainly consists of alternating 3-linked β-D-galactopyranose and 4-linked α-D-galactopyranose or 4-linked 3,6-anhydro-α-D-galactopyranose, forming the repeating disaccharide unit of the structure.[18,19] Carrageenans are divided into six different types, differing from each other in terms of number and placement of the sulfate ester groups. Among these types, the most commercially important ones are iota (ι)-, kappa (κ)- and lambda (λ)-carrageenan[18], which are widely used in food industry as wells as in products such as cosmetics, pharmaceuticals, and in printing. This is due to their gelling, thickening and stabilizing abilities, where both ι- and κ-carrageenan form thermo-reversible gels with textures ranging from soft and elastic to brittle and firm.[16,18–20] All carrageenans are soluble in water and the extent of their solubility depends on the number of sulfate groups, where κ-carrageenan has one, as well as on the cation

associated with them. When utilizing carrageenans for gelation, cations must be present to make the gelation successful. As κ-carrageenan undergoes gelation there will first be a structural coil-to-helix transition upon cooling and subsequently an aggregation between helices. Both of these processes are cation-dependent.[18,21,22] For κ-carrageenan, ions such as K^+, Na^+, Ca^{2+}, Li^+ and Mg^{2+} can induce this process, where for example K^+ has a much greater ability to induce the gelation compared to Na^+.[16] However, the choice of cation is not always straightforward as it also affects the solubility of carrageenan as well as many properties of the gel, such as strength and texture.[18,23,24]

One of the applications for tubular calcium phosphate structures already being explored is their possible use as cellular scaffold for bone tissue engineering[10,11,13] as well as coatings for solid-phase microextraction.[25,26] Interestingly, κ-carrageenan is also recognized within the field of bone tissue engineering as promising candidate for developing composites.[21,27] Exploring the possibility of growing chemical gardens from κ-carrageenan hydrogels in the form of calcium phosphates could therefore be seen as an excellent opportunity to explore this field further. In our previous preliminary study, we showed that calcium phosphate gardens can indeed be grown from κ-carrageenan hydrogel/liquid interfaces.[14] Two systems, with phosphate- or calcium-based hydrogels, result in very different tubular structures. For instance, we have noticed a significant difference in macrostructures (length and shape). Further, the phosphate-based system gave rise to structures with some crystallinity while the structures of the calcium-based system remained amorphous. However, the time and pH factors were not addressed in our previous study but are considered to be important.[12,13,15,28] Thus, it would be beneficial to gain more control of the growth process and the tubular structures by investigating the effect of these factors in our systems further.

In the present study, a calcium-based hydrogel with a phosphate counterion solution (Ca-gel) and a phosphate-based hydrogel with a calcium counterion solution (P-gel) were investigated

more thoroughly. The manufacturing processes of the chemobrionic systems were optimized to make them less time consuming. The pH environments of the two systems were investigated to gain more knowledge of possible differences in the systems. In the present study we have also investigated if and, in that case what, kind of crystalline phases can be obtained in the Ca-gel system. Further, the obtained structures were assessed more thoroughly than before regarding their microstructure, crystallinity and thermal behavior. Additionally, we have investigated how the maturation time in the parent counterion solution affects microstructural and compositional properties of the tubular structures in both systems.

RESULTS AND DISCUSSION

Characteristics of the growth process

Both the Ca-gel and P-gel systems exhibited tubular growth from the gel/liquid interface, but with differences in their macrostructure and length apparent to the naked eye. Both differences were visible already after 1 h (Figure S1A and S1B). The observed growth in length for the P-gel tubes stopped within a few hours, while the Ca-gel tubes continued to grow for an extended period. The P-gel tubes thus remained fully immersed in the liquid, while the Ca-gel tubes reached all the way to the surface of the counterion solution. Thereby resulting in structures stemming from the tubes assembling along the surface (Figure 1A and Figure S2). Time-lapse videos of the first 2 h of the growth process can be found in the Supporting Information (SI).

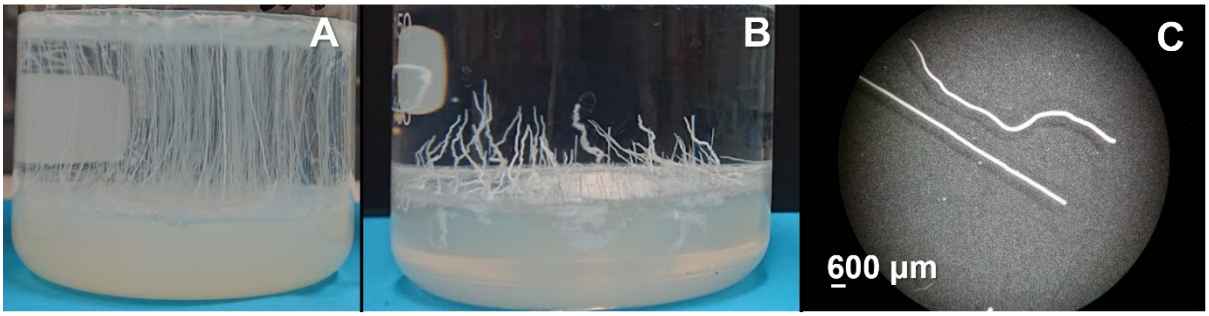

Figure 1. The growth in 1 day of Ca-gel (A) and P-gel (B) showcased in 250 ml beakers with a diameter of 7 cm; a microscopy images (C) of a P-gel tube (top) and a Ca-gel tube (bottom) after 1-day growth.

The tubes did not only differ in length, but they were also different in shape. While both tube types grew upwards, the P-gel tubes had clear kinks giving them a more crooked structure and the tube from a Ca-gel system is completely straight (Figure 1C). This difference in macrostructure can be attributed to the speed of the growth process.[28] As the Ca-gel tubes grew substantially faster than the P-gel tubes, more solution would be jetted with each time and the semipermeable membrane formed on the tube after each ejection of fluid would not grow as thick. In this case, the large osmotic pressure would break the tubes in the top when more calcium solution from the hydrogel was ejected into the phosphate solution. The P-gel tubes, however, grew more slowly and thus the semipermeable membrane grew thicker and was subsequently more likely to break at random places as the phosphate solution from the hydrogel would be ejected.

The pH difference between the hydrogel and the layering solution is one of the factors affecting the growth process in the two systems.[6,29] The change in pH with time of both the hydrogel and the counterion solution during the first hour after layering is shown in Figure 2. After an initial increase in pH from about 7 to 10.7 in the Ca-gel hydrogel, the difference in pH between the hydrogel and its counterion solution (pH 12.8) was maintained during the entire observed period (ΔpH ~2.1). Meanwhile, for the P-gel system, the pH of the counterion solution

changed very rapidly and reached the same pH value as the hydrogel within 45 min. As there is no pH difference between the hydrogel (pH 11.3) and the counterion solution (pH 11.3 at 44 min) anymore, there is also no driving force of the growth process.[15] This can at least partly explain the limited growth period of the P-gel.

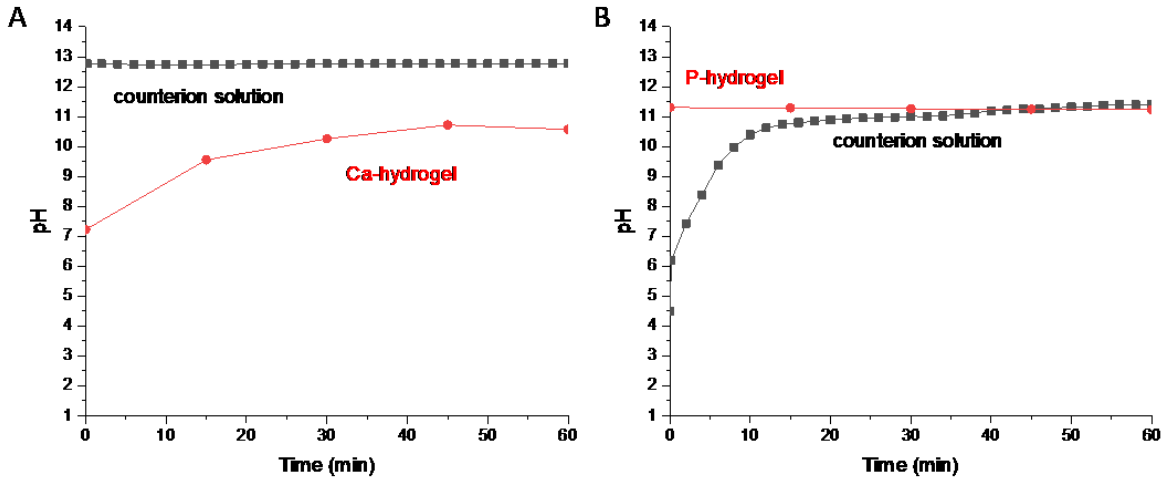

Figure 2. Changes in pH for the hydrogels and counterion solutions in the Ca-gel (A) and P-gel (B) systems during the first hour. The pH of the hydrogels was measured at four different places and the mean values were plotted.

The graph in Figure 2B illustrates the rapid change in pH of the P-gel counterion solution as soon as it encounters the hydrogel. κ-carrageenan hydrogels are known to exhibit syneresis, which is a process where fluid is spontaneously released from the gel.[30] Presumably, this would likely push both OH^- and PO_4^{3-} ions out of the hydrogel, since these ions are not fixed in the hydrogel matrix by the polysaccharide. This is contrary to the Ca^{2+} ions, which are fixed in the Ca-hydrogel matrix as they are participating in the buildup of the hydrogel itself. Thus, the mobile PO_4^{3-} ions in the P-gel system would form a thicker and coarser membrane on top of the hydrogel in contact with the counterion solution, compared to the more strongly bonded Ca^{2+} ions in the Ca-gel system. Hypothetically, a thicker (and perhaps impermeable) membrane formed on top of the P-gel which can hinder the movement of solvent (water molecules) from

liquid phase to the gel phase to build up pressure. We therefore assume a low osmotic pressure within the P-gel, leading to shorter tubes. Further, even though the κ-carrageenan forms a complex with the Ca^{2+} ions, we do not expect all the Ca^{2+} ions present in the aqueous solution used for making the gel to be bound in the matrix. Additionally, as some of the ions are bound, we would expect the solution being jetted from the gel/liquid interface to have a lower density, thereby shooting further up into the layering solution. Thereby still leading to longer tubes in the Ca-gel system

Morphology of the tubes

SEM micrographs (Figure 3) of cross-sections of the tubes revealed different kinds of morphologies at three main regions, i.e., the exterior of the tubes, the wall of the tubes, and the interior of the tubes. Visual examples of tubes after 1 day in counterion solution (left column) and 28 days in counterion solution (right column) are given in Figure 3. The SI includes SEM micrographs of both kind of tubes at all four investigated time points (Figure S3).

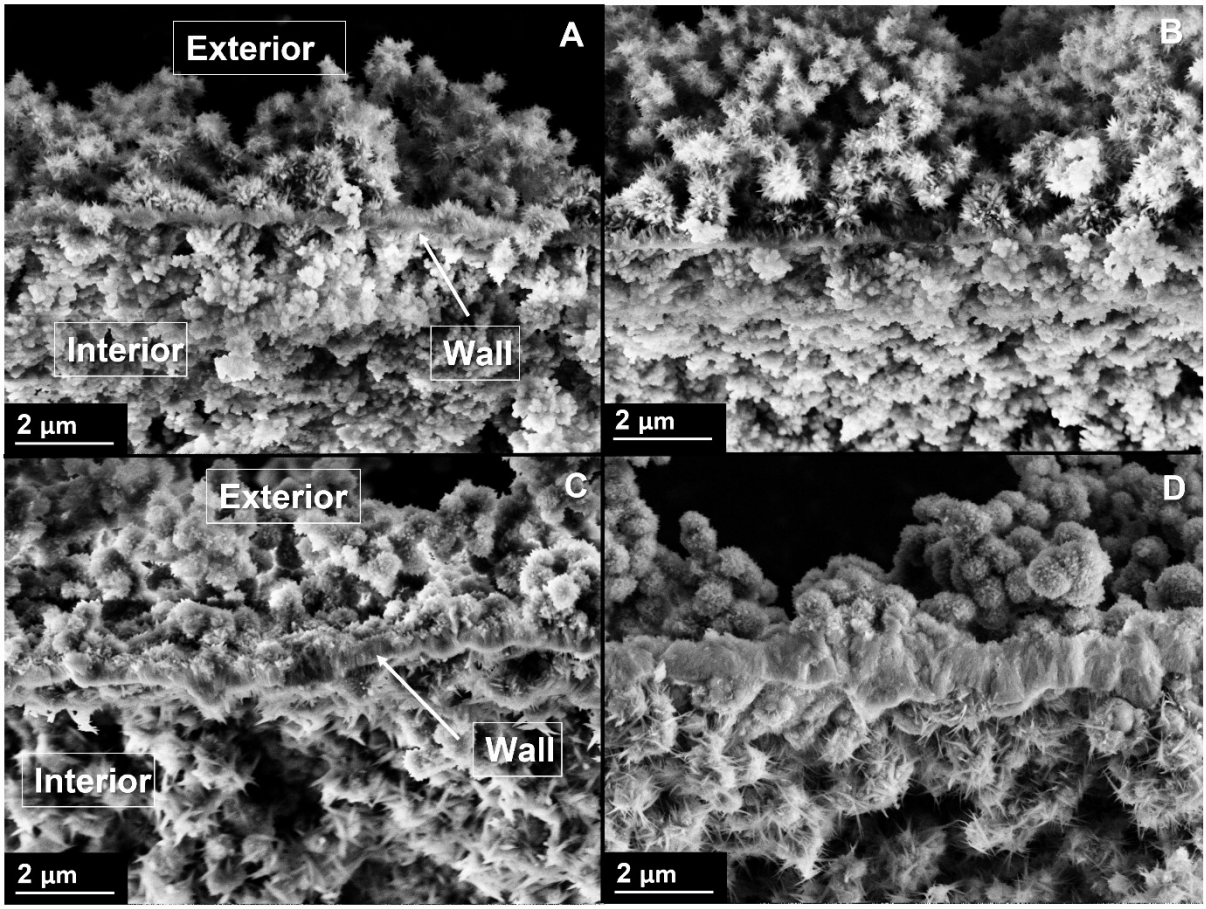

Figure 3. Cross-sectional SEM images of tubes that have been kept in counterion solution for 1 day or 28 days: Ca-gel 1 day (A), Ca-gel 28 days (B), P-gel 1 day (C) and P-gel 28 days (D). The magnification is 10k.

When comparing the SEM micrographs of the two types of tubes, some differences in morphology could be observed; for instance, the Ca-gel tubes had much thinner walls than the P-gel tubes. The thickness of the P-gel tube walls varies from approx. 0.5-3 µm (Figure S3E-S3H). Furthermore, the P-gel tube walls exhibited a fiber-like structure (Figure 3B&3D), while the Ca-gel tube walls were too thin to distinguish any features of. The higher pH of the counterion solution in the Ca-gel system is likely to give more amorphous and gelatinous structures.[28,31] Together with the higher growth rate of the tubes this would stretch the semipermeable membrane created during the growth much more than in the P-gel system, leading to thinner, less crystalline walls. Furthermore, the tubes in both gel systems were

slightly heterogeneous (as suggested by the photographs in Figure 1), which could explain some of the variations observed in the SEM micrographs.

The exterior and interior regions of both the Ca-gel and P-gel tubes exhibited two main kinds of structure units, a granular and a needle-like. The granular structure was also found on the interior of both kinds of tubes but is smaller for the Ca-gel tubes. For the P-gel tubes, also the interior exhibited needle-like structures on top of the granules, but longer and wider than those observed on the exterior surfaces, i.e., granular in nature and the granules were covered with thinner needles for both the Ca-gel tubes and the P-gel tubes. In case of the Ca-gel tubes, the granules were smaller and the needles longer in comparison to the P-gel tubes. Similar results were found in the AFM images captured from the exterior surfaces (Figure 4).

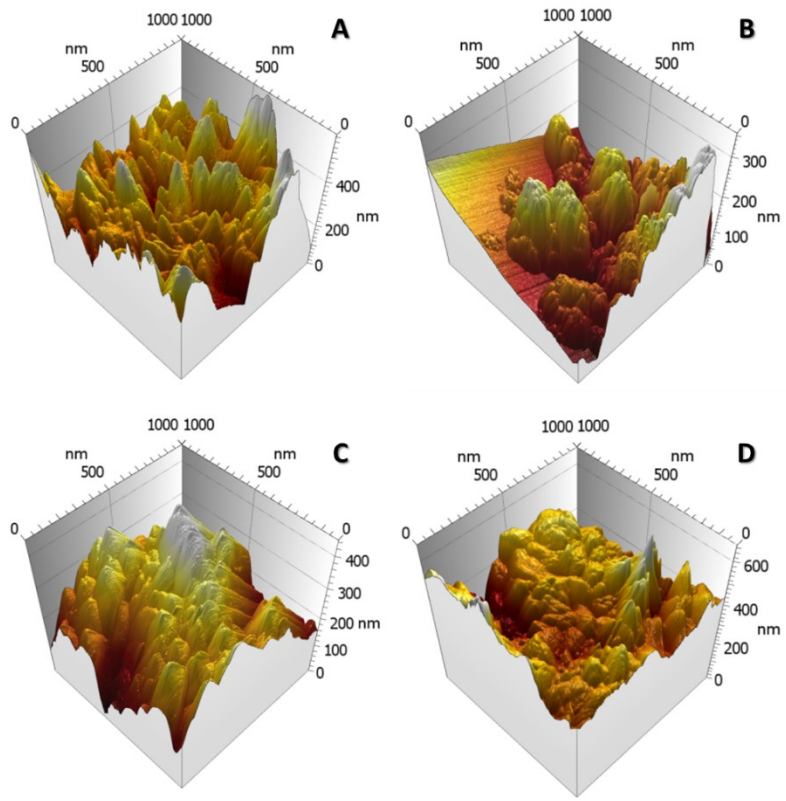

Figure 4. 3D-rendered AFM images (1×1 μm) of tubes kept in counterions solutions for 1 day or 28 days: Ca-gel 1-day (A), Ca-gel 28 days (B), P-gel 1-day (C) and P-gel 28 days (D) tubes.

When the four kinds of tubes were also analyzed for their nanoscale roughness, they were found to be very heterogenous, as can be seen from their large standard deviations (Table S1 and S2). At 1 day, the Ca-gel tubes were significantly ($p>0.9$) rougher than the P-gel tube in terms of S_a, S_q, S_{dr}, S_{ds}, and S_{ku} values. Over the course of the 28-day maturation process, the nanoscale roughness of the Ca-gel did not change significantly except for S_a ($p=0.9$ level), which decreased from approx. 63 nm to 31 nm. However, the P-gel showed a significant increase in S_a at $p=0.95$ and S_q at 0.9 and an increased S_{al} ($p=0.95$) as well as a decreased S_{ku} ($p=0.99$).

An analysis of the DMT modulus of the surfaces obtained with PeakForce™ showed large areal variations in the modulus imaged for all samples except the 28 days P-gel tube. The 1-day Ca-gel tube was the softest of the samples, averaging at approx. 14 MPa (range of peak points 3 MPa–44 MPa). The 28 days samples were stiffer, on average approx. 42 MPa (1.5 MPa–141 MPa). These distributions also had a clearly positive skew in some images, showing local stiffness moduli even up to the GPa range. Overall, the P-gel tubes were stiffer than the Ca-gel tubes. The 1-day P-gel tube had an average stiffness modulus of approx. 372 MPa (18 MPa–1.14 GPa), and the 28 days P-gel tube approx. 258 MPa (186–377 MPa). At both 1 day and 28 days of maturation, tubes also exhibited a positive skewness, often reaching the 1–10 GPa range for the 1-day P-gel and up to 0.6–1.1 GPa for the 28-day P-gel. The positive skewness indicates a small distribution of stiffer regions in the imaged areas, possibly more densely packed or more crystalline. The higher stiffness modulus could indicate that the P-gel tubes are denser or more crystalline than the Ca-gel tubes.

Structural analysis and thermal behavior of the tubes

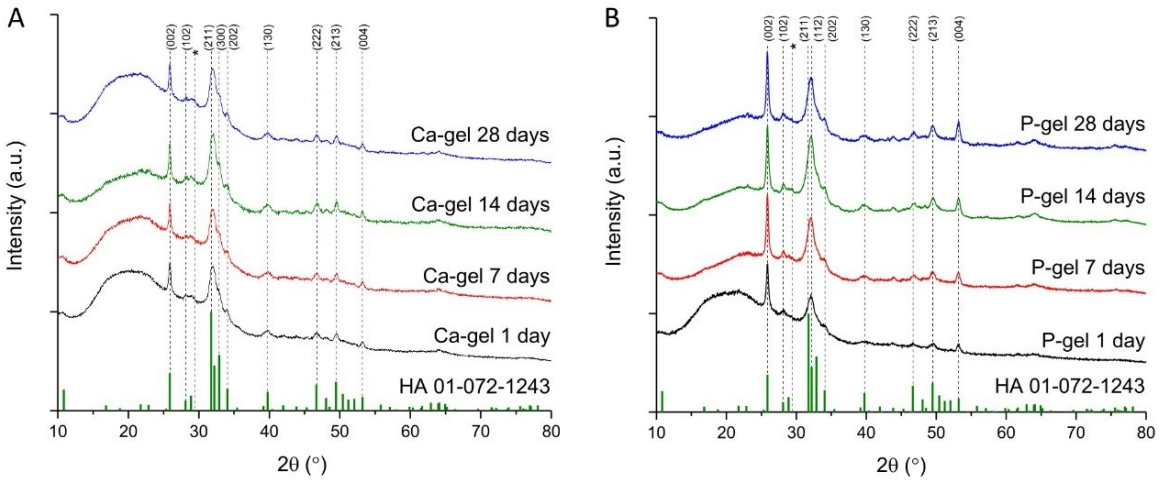

Figure 5. PXRD patterns of Ca-gel tubes (A) and P-gel tubes (B). Reference pattern of hydroxyapatite (JCPDS #01-072-1243) in green and the most intensive peak of calcite marked with * (JCPDS #00-005-0586).

The obtained PXRD patterns of all types of tubes can be seen in Figure 5. The most prominent peaks in the PXRD patterns were found at 25.9° and ~32°, where the second peak consists of several reflections combined. The XRD data of all samples matches well with the reference pattern of hydroxyapatite (HA, JCPDS #01-072-1243). However, it should be noted that also calcium-deficient hydroxyapatite (CDHA, JCPDS #00-46-0905) would give an almost identical XRD pattern. Even though dominating forms of phosphate are PO_4^{3-} at pH 13 and HPO_4^{2-} at pH 11 (Figure 2) in the counter solutions of Ca-gel and P-gel systems, respectively[32], hydroxyapatite is the main precipitation product which could be explained using the predominance area diagram of calcium phosphates[33]. In addition, a broad hump at 12–35° was visible for the samples having spent less time in the counterion solution, and it was also more evident for the Ca-gel samples compared to the P-gel samples. This hump can either be attributed to κ-carrageenan (Figure S5), the sample holder (Figure S5), amorphous calcium phosphate (ACP)[34], or a combination of these. In our previous study, we observed that Ca-gel tubes which had spent only 3 h in counterion solution consisted of amorphous calcium

phosphate[14]. We therefore assume that at least the Ca-gel tubes have been amorphous at some point. The presence of κ-carrageenan in some of the tubes was also indicated by trace amounts of sulfur, which could be found in the 7 days and 14 days Ca-gel tubes according to our EDS data (Table S3).

While the peaks in the PXRD patterns for both P-gel tubes and Ca-gel tubes appeared at the same angles when comparing the samples of the two systems, the relative intensities of the two highest ones (at 25.9° and 32°) differ. This indicates a difference in the preferred orientation of the crystal structure for the P-gel tubes, seen as pronounced reflections at 25.9°, 32.2° and 53.2°, corresponding to the (002), (112) and (004) reflections of HA. The (002) and (004) reflections can be attributed to a layered structure as the planar growth directions would result in a similar reflection enhancement. This was supported by the SEM micrographs (Figure 3B), where the P-gel tubes had a distinctively thicker wall consisting of a fiber-like structure.

The more mature samples of both the Ca-gel tubes (14 and 28 days) and P-gel tubes (7, 14 and 28 days) had additional peaks at 29.4° (indicated with an asterisk in Figure 5), 39.4° and 43.1° that fit well with the pattern for calcite ($CaCO_3$, JCPDS #00-005-0586). These peaks were most clearly visible in the 14 days P-gel sample and 28 days Ca-gel sample (P-gel sample also had visible peaks at 23.0° and 36.0° that fit with the calcite pattern). When analyzing the structures appearing on the surface of the Ca-gel counterion solution (Figure S1), the intensity of these calcite peaks was even more evident (Figure S7). As the peaks are most intense in the structure on the surface of the counterion solution we expect that the calcite formation is due to carbon dioxide from the air dissolving into the solutions. In addition, the source of carbonate cannot be from carrageenan as there is no relevant compound found in the PXRD pattern of carrageenan (Figure S5).

The gradual change observed in our PXRD patterns, especially the peaks around 50–55° of the P-gel tubes, is consistent with crystallization of HA, shown for example by Rollin-Martinet

et al.[35] However, both HA and CDHA are usually poorly crystalline when unsintered.[36] In addition, ACP tends to slowly recrystallize into compounds with better crystallinity such as CDHA when left in its parent solution.[34,36] It is possible that this process is slowed down further in our case since one of the required ions is initially locked inside the gel (especially in the case of the Ca-gel system). Overall, the P-gel tubes seem to have a more crystalline structure than the Ca-gel tubes.

Thermogravimetric analysis data of the samples is shown in Figure 6. The total mass loss (18.2–21.5 wt%) was larger for all the Ca-gel samples in comparison to their corresponding P-gel samples (12.9–16.8 wt%). Details of the mass decrease in different temperature regions can be found in Table S4. All the investigated tube samples showed three main stages of mass loss. Temperatures for the maximum DTG signals (DTG_{max}) for the mentioned stages are also included in Table S4. As references, TG and DTG curves of the neat κ-carrageenan powder used in the hydrogels, as well as of the top layer formed on the Ca-gel counterion solution after 1 day and 28 days (Figure S2) are shown in Figure S8. The top layer of the Ca-gel solution showed an increase in mass loss between 30–50 °C and a larger mass loss step between 600–750 °C. The neat κ-carrageenan showed five distinct stages of mass loss in the temperature ranges 40–120 °C, 160–210 °C, 210–290 °C, 290 °C–550 °C, and 660–750 °C.

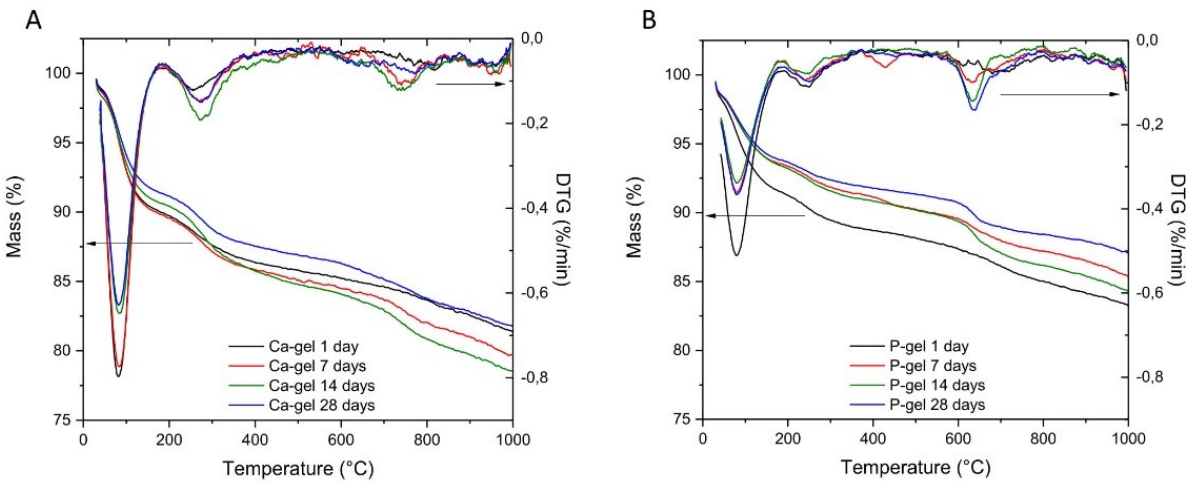

Figure 6. TG and DTG curves for Ca-gel samples (A) and P-gel samples (B), showing measurements of 1- (black), 7- (red), 14- (green), and 28-day (blue) samples.

The first mass loss stage, observed between 30–180 °C for all samples, corresponds to the loss of physisorbed water.[37] The mass loss was greater for the Ca-gel samples (8.2–9.7 %). In addition, the 1-day P-gel sample (7.9 %) showed significantly more mass loss than the rest of the P-gel samples (5.6–6.1 %). This can possibly be explained by the more amorphous structure of the Ca-gel samples and the 1-day P-gel sample compared to the rest of the samples. Amorphous structures have higher surface areas where the physisorption can take place. Thus, the amount of physisorbed water decreases with a higher degree of crystallinity of the material.[37,38] These results are in line with the observations on sample crystallinity from the PXRD patterns.

A second mass loss step was observed between 180–330 °C for both kinds of tubes. In this temperature range the mass loss for the Ca-gel samples (2.6–3.6 %) is larger and more pronounced than for the P-gel samples (1.2–1.8 %), where a clear decrease is visible especially for the 14-day Ca-gel sample (3.6 %). The mass loss in this region corresponds to loss of structural water (between 200–400 °C), but also decomposition of organic molecules like polysaccharides (starting from 200 °C).[37–39] In the case of the Ca-gel samples, the behavior

above 250 °C resembled that of the neat κ-carrageenan powder (Figure S8). The slight shift of the mass loss of the Ca-gel samples towards higher temperature when compared to that of the neat κ-carrageenan can be attributed to the interaction of κ-carrageenan and calcium phosphate due to the formation of hydrogen bonds between hydroxyapatite and the sulfonic groups of κ-carrageenan, giving an increase in thermal stability.[21,38]

A third stage of mass loss was observed between 600–660 °C for the P-gel tubes (except for the 1-day grown tubes) and 690–780 °C for the Ca-gel tubes. Between 600–800 °C events such as further decomposition of κ-carrageenan, decomposition of calcium carbonate, volatilization of carbonate ions or decarbonation of carbonated hydroxyapatite (CAP) take place.[40–43] The mass loss observed for the P-gel systems corresponds to the loss of carbonate and correlates well with the presence of calcite peaks in the PXRD patterns. The 14- and 28-day Ca-gel samples showed minor mass loss in this region. This behavior is supported by the PXRD pattern of the 28-day Ca-gel top layer sample (Figure S8), where clear calcite peaks could also be observed. The mass loss step for the Ca-gel samples between 690 and 780 °C (which was not present in any of the P-gel samples), corresponds to the further decomposition of κ-carrageenan. A resemblance to this behavior can be seen in the mass loss of the neat κ-carrageenan (Figure S8), albeit with a shift to higher temperatures due to the stabilizing interaction of the HA in Ca-gel samples. The obtained EDS data (Table S3) confirmed traces of sulfur (found in κ-carrageenan) in the 7 days and 14 days Ca-gel samples. This suggests that these two samples contained more κ-carrageenan than the other samples, in line with the fact that these two samples exhibit the largest mass loss in this temperature range.

CONCLUSIONS

We have investigated two chemobrionic systems where the chemobrionic structures were grown as tubes from an interface between a κ-carrageenan hydrogel and a counterion solution.

Further investigation of our two systems, revealed differences in pH changes during the initial growth period, where a pH difference between the hydrogel and the counterion solution was observed for a longer time period in the Ca-gel system. This gave rise to tubes that were longer and straighter as well as more numerous compared to what was observed in the P-gel system.

Characterization of the various tubes showed differences in wall size and wall structure (observed with SEM and AFM), crystalline phases (PXRD and AFM), and in the thermal decomposition behavior (TG and DTG). Based on this information, we can draw some conclusions on differences in the morphologies and structures between the two systems. First, the tubes from both systems were crystalline to some degree, and that the crystallization process continued when leaving the tubes for a longer time in their parent counterion solution. The P-gel tubes appeared to be more crystalline than the Ca-gel tubes. However, based only on the PXRD data it was not possible to distinguish if the observed phase was HA or CDHA. PXRD data combined with TGA and EDS results suggest that all Ca-gel tubes contained some κ-carrageenan, and that the 14 and 28 days Ca-gel samples additionally contained trace amounts of calcite. In the case of the P-gel tubes, calcite was found in the 7–28-day samples, while no indication of remnant κ-carrageenan was found in any of the P-gel samples.

EXPERIMENTAL SECTION

Materials

Trisodium phosphate (tert) dodecahydrate ($Na_3PO_4 \cdot 12H_2O$), calcium chloride dihydrate ($CaCl_2 \cdot 2H_2O$), hydrochloric acid (HCl) 37%, and sodium hydroxide (NaOH), all analytical grade, were obtained from Merck (Germany). κ-carrageenan powder (food-grade) produced by Specialingredient (UK) was purchased via Amazon. Ethanol (99.5 %) was obtained from Altia (Finland). All chemicals were used as received without any further purification.

Preparation of hydrogels

The procedure for preparing the hydrogels is adapted from the procedure developed in our previous paper.[14] In short, the hydrogels that were used in this study were prepared by adding 1.5 wt% κ-carrageenan into 0.1 M solutions of calcium chloride (pH 4.5) or tri-sodium phosphate (pH 12.9) at room temperature. The pH of the salt solutions was adjusted beforehand using HCl or NaOH. After manually stirring the mixtures, the dispersions were heated and stirred simultaneously until clearly solubilized solutions were obtained and a final temperature between 65–75 °C was reached. The solutions containing calcium chloride and tri-sodium phosphate were heated for 30 min and 10 min, respectively. At the end of the heating, 5 ml of deionized (DI) water was added, and the gel solutions were stirred for an additional minute. After this, the viscous solutions were transferred into beakers and left standing at room temperature for 15 min for cooling down and setting.

Growth of tubes

Tubes were grown from the hydrogel/liquid interface created by layering the corresponding counterion solution on top of the hydrogel (at a 2:5 volume ratio of hydrogel to counterion solution). The Ca-gel tubes were grown from the hydrogel/liquid interface by layering a calcium hydrogel with a solution of 0.05 M trisodium phosphate (pH 12.9), and the P-gel tubes were grown by layering a phosphate hydrogel with a solution of 0.1 M calcium dichloride (pH 4.5). The beakers were covered with parafilm and an upside-down, weighted Petri dish and were thereafter left without disturbances on a stable surface for the duration of the growth and maturing process.

Investigation of the growth process

The growth of the tubes was documented in a time-lapse video with a 60-second interval using a GoPro Hero 7 Black camera (GoPro, Inc, USA). The captured videos can be found in the Supporting Information (SI) and are played at a rate of 30 frames per second.

The pH of the layered counterion solutions as well as the hydrogels was measured using a Metrohm 744 pH Meter (Metrohm Ltd., Switzerland). The pH of the counterion solutions was measured using a solitrode combined glass electrode during the first 60 min of the growth process and the reading was recorded using a GoPro Hero 7 Black camera. The pH probe was placed approximately 1 cm above the hydrogel surface during the entire measurement. Afterwards, the pH was logged for every two minutes. The pH of the hydrogels was measured using a spearhead electrode with a gel electrolyte. To avoid damaging the electrode as well as disturbances from the counter ion solution, the pH measurements of the hydrogels were performed at room temperature and after removing the counterion solution. The hydrogel surface was rinsed with water and gently dabbed dry with paper

before pH measurement. The measurements were done at growth time of 0, 15, 30, 45 or 60 min, where each time point was measured on a separate gel from the same batch (5 gels in total).

Characterization of the tubes

The tubes were transferred from the beaker to a Petri dish with a plastic pipette. They were rinsed twice with distilled water and then twice with ethanol (99.5%) to remove possible additional material (e.g., unreacted precursors and non-tubular products from reactions at the gel/liquid interface) or excess solution. The tubes were finally transferred to another Petri dish and left in room temperature overnight to dry.

The tubes were photographed during different stages of the growth process with a Sony Xperia XZ2 Compact 19-megapixel mobile phone camera (Sony, Japan). Photographs of washed and dried tubes were taken using the Olympus SZX12 stereo microscope (Olympus Corporation, Japan) with a Nikon Coolpix camera (Nikon, Japan).

The morphology of the tubes was studied on intact tubes from the collected samples using scanning electron microscopy (SEM) and atomic force microscopy (AFM). For the SEM analysis, the collected tubes were placed on double-sided sticky carbon tape and sputtered with Au. The analysis was performed using a LEO Gemini 1530 SEM (Zeiss Microscopy GmbH., Germany). The instrument was additionally equipped with a Thermo Scientific UltraDry silicon drift detector (SDD) EDS-system, which was used for elemental analysis of the samples.

The exterior surface of the 1 day and 28 days tubes of both systems were imaged with a Nanoscope V MultiMode 8 AFM (Bruker, USA) using PeakForce Quantitative Nano-mechanical (QNM)™ mode. The cantilevers chosen were of type NSG03 (NT-MDT, Russia) having a typical spring constant (k) of 1.74 N/m (0.35-6.1 N/m) and a typical tip radius of 6 nm (<10 nm) as given by the manufacturer. The used cantilevers were characterized to be in the *k*-range 1.01–4.12 N/m. Captured images were of 1×1 μm size, having a 512×512-pixel resolution. Shown 3D and 2D topographical data have been levelled by a plane tilt and also a 2nd order plane fit. PeakForce™ tapping uses the DMT (Derjaguin, Muller, Toporov) modulus, which also accounts for elastic responses in the investigated surface.[44] The stiffness analysis was done as a histogram analysis comparing average peak positions of a minimum of 5 images. In addition to the stiffness modulus, a set of roughness parameters were investigated for the surfaces. These parameters were height parameters (S_a and S_q), spacing between features (S_{al}), surface area ratio (S_{dr}), summit density (S_{ds}), peak or valley dominance (skewness, S_{sk}) and surface peakedness (kurtosis, S_{ku}). The used parameters are described in the SI. Roughness parameters, topographical image renders, as well as the PeakForce stiffness modulus maps were obtained with MountainsSPIP® Academic (Version: 9.0.9733, DigitalSurf, France). Statistical differences between the roughness parameters of surfaces were investigated with

a one-way ANOVA analysis done using LibreOffice. Stars indicate statistical differences at p=0.9 level (one star), p=0.95 level (two stars), and p=0.99 level (three stars).

Prior to X-ray diffraction (XRD) and thermogravimetric analysis (TGA) measurements, all samples were ground into fine powder in a mortar to get representative samples of the bulk compositions. A Bruker D8 Discover X-ray diffractometer (Bruker-AXS, Germany) with a scintillation detector and copper Kα radiation (λ = 1.54 Å) was used to obtain powder X-ray diffraction (PXRD) patterns in the 2θ range of 10° to 80° with a step size of 0.04°. Prior to measurements, the powders were compressed onto glass slides with double-sided sticky tape, from which the measurement was then performed. The obtained patterns were matched against patterns from the ICDD database (2010 RDB PDF-2) using the EVA 2 software (Version: 16.0) by Bruker-AXS (Germany). A Netzsch STA 449 F1 Jupiter TGA (Netzsch, Germany) was used for the TGA measurements and was employed under N_2 inert atmosphere from 30 to 1000 °C at a heating rate of 5 °C/min. The N_2 flow rate was kept at 20 mL/min. Prior to measurements, the dry samples were kept in vacuum and 2-10 mg of the dry samples were transferred to alumina crucibles. Derivative thermogravimetric (DTG) curves were plotted to help with detecting significant weight changes of the samples. The TGA data was analyzed with the Netzsch Proteus Thermal Analysis Software (Version: 5.2.1).

ASSOCIATED CONTENT

Supporting information

Additional photographs of tubular growth, additional experimental details and results (AFM) PXRD patterns of reference samples and Ca-gel top layer samples, TG and DTG curves of reference samples and Ca-gel top layer samples, EDS data (Supporting information.PDF)

Time-lapse video of tubular growth of the Ca-gel system (Video 1)

Time-lapse video of tubular growth of the P-gel system (Video 2)

AUTHOR INFORMATION

Corresponding author

Tan-Phat Huynh - Laboratory of Molecular Science and Engineering, Åbo Akademi University, FI-20500, Turku, Finland

Email: tan.huynh@abo.fi

Author

Anna Fogde – Laboratory of Molecular Science and Engineering, Åbo Akademi University, FI-20500, Turku, Finland

Department of Mechanical and Materials Engineering, University of Turku, FI-20014 Turku, Finland

Emil Rosqvist – Laboratory of Molecular Science and Engineering, Åbo Akademi University, FI-20500, Turku, Finland

Trung-Anh Le – Laboratory of Molecular Science and Engineering, Åbo Akademi University, FI-20500, Turku, Finland

Jan-Henrik Smått – Laboratory of Molecular Science and Engineering, Åbo Akademi University, FI-20500, Turku, Finland

Thomas Sandberg – Laboratory of Molecular Science and Engineering, Åbo Akademi University, FI-20500, Turku, Finland

Author Contributions

The manuscript was written through contributions of all authors. All authors have given approval to the final version of the manuscript.

Notes

The authors declare no competing financial interest.

ACKNOWLEDGMENT

ER acknowledges the Jane and Aatos Erkko Foundation for funding the project ABC Health

(Anti-Bacterial Channelling from Waste to Human Health). TPH would like to acknowledge the contribution of the European COST Action CA17120 supported by the EU Framework Programme Horizon 2020, and the Academy of Finland (Grant No. 323240). TAL acknowledges the support from Magnus Ehrnrooth foundation and Finnish Society of Sciences & Letters.

KEYWORDS: calcium phosphate • carrageenan • chemical gardens • hydrogels • tubular structures

REFERENCES

[1] O. Steinbock, J. H. E. Cartwright, L. M. Barge, *Phys. Today* **2016**, *69*, 44–51.

[2] J. H. E. Cartwright, J. M. García-Ruiz, M. L. Novella, F. Otálora, C. J. H. E., G.-R. J. M., N. M. L., O. F., *J. Colloid Interface Sci.* **2002**, *256*, 351–359.

[3] T. H. Hazlehurst, *J. Chem. Educ.* **1941**, *18*, 286–289.

[4] M. Matsuoka, *J. Chem. Educ.* **2017**, *94*, 621–625.

[5] B. Z. Shakhashiri, *Chemical Demonstrations : A Handbook for Teachers of Chemistry. 3*, Univ. Of Wisconsin, Madison, **1989**.

[6] L. M. Barge, S. S. S. Cardoso, J. H. E. Cartwright, G. J. T. Cooper, L. Cronin, A. De Wit, I. J. Doloboff, B. Escribano, R. E. Goldstein, F. Haudin, D. E. H. Jones, A. L. Mackay, J. Maselko, J. J. Pagano, J. Pantaleone, M. J. Russell, C. I. Sainz-Díaz, O. Steinbock, D. A. Stone, Y. Tanimoto, N. L. Thomas, *Chem. Rev.* **2015**, *115*, 8652–8703.

[7] S. S. S. Cardoso, J. H. E. Cartwright, J. Čejková, L. Cronin, A. De Wit, S. Giannerini, D. Horváth, A. Rodrigues, M. J. Russell, C. I. Sainz-Díaz, Á. Tóth, *Artif. Life* **2020**, *26*, 315–326.

[8] M. Zouheir, M. Zniber, S. Qudsia, T. P. Huynh, *Sensors Actuators, A Phys.* **2021**, *319*, 112541.

[9] M. Zouheir, T. Le, J. Torop, K. Nikiforow, M. Khatib, O. Zohar, H. Haick, T. Huynh, *ChemSystemsChem* **2021**, DOI 10.1002/syst.202000063.

[10] E. A. B. Hughes, M. Chipara, T. J. Hall, R. L. Williams, L. M. Grover, *Biomater. Sci.* **2020**, *8*, 812–822.

[11] E. A. B. B. Hughes, S. C. Cox, M. E. Cooke, O. G. Davies, R. L. Williams, T. J. Hall, L. M. Grover, *Adv. Healthc. Mater.* **2018**, *7*, 1701166.

[12] C. J. Steenbjerg Ibsen, B. F. Mikladal, U. Bjørnholt Jensen, H. Birkedal, C. J. Steenbjerg Ibsen, B. F. Mikladal, U. Bjørnholt Jensen, H. Birkedal, *Chem. - A Eur. J.* **2014**, *20*, 16112–16120.

[13] E. A. B. Hughes, R. L. Williams, S. C. Cox, L. M. Grover, *Langmuir* **2017**, *33*, 2059–2067.

[14] A. Fogde, S. Qudsia, T. Le, T. Sandberg, T. Huynh, *ChemSystemsChem* **2021**, *3*, DOI 10.1002/syst.202000064.

[15] E. A. B. Hughes, O. Jones-Salkey, P. Forey, M. Chipara, L. M. Grover, *ChemSystemsChem* **2021**, *3*, DOI 10.1002/syst.202000062.

[16] W. R. Blakemore, A. R. Harpell, in *Food Stabilisers, Thick. Gelling Agents* (Ed.: A. Imeson), Wiley-Blackwell, Oxford, UK, **2009**, pp. 73–94.

[17] Y. Freile-Pelegrín, J. A. Azamar, D. Robledo, *https://doi.org/10.1080/10498850.2010.541590* **2011**, *20*, 73–83.

[18] V. L. Campo, D. F. Kawano, D. B. da Silva, I. Carvalho, *Carbohydr. Polym.* **2009**, *77*, 167–180.

[19] J. Necas, L. Bartosikova, *Vet. Med. (Praha).* **2013**, *58*, 187–205.

[20] J. N. BeMiller, in *Carbohydr. Chem. Food Sci.*, Elsevier, **2019**, pp. 279–291.

[21] A. L. Daniel-Da-Silva, A. B. Lopes, A. M. Gil, R. N. Correia, *J. Mater. Sci.* **2007**, *42*, 8581–8591.

[22] E. R. Morris, D. A. Rees, G. Robinson, *J. Mol. Biol.* **1980**, *138*, 349–362.

[23] M. Rinaudo, *J. Intell. Mater. Syst. Struct.* **1993**, *4*, 210–215.

[24] M. Robal, T. Brenner, S. Matsukawa, H. Ogawa, K. Truus, B. Rudolph, R. Tuvikene, *Food Hydrocoll.* **2017**, *63*, 656–667.

[25] Z. Wang, P. Jin, S. Zhou, X. Wang, X. Du, *Anal. Methods* **2018**, *10*, 3237–3247.

[26] J. Wang, B. Ni, W. Li, J. Sun, Y. Tao, L. Chen, *J. Chromatogr. A* **2021**, *1653*, 462438.

[27] I. Y. Kim, R. Iwatsuki, K. Kikuta, Y. Morita, T. Miyazaki, C. Ohtsuki, *Mater. Sci. Eng. C* **2011**, *31*, 1472–1476.

[28] M. Tanahashi, K. Kamiya, T. Suzuki, H. Nasu, *J. Mater. Sci. Mater. Med.* **1992**, *3*, 48–53.

[29] E. A. B. Hughes, T. E. Robinson, R. J. A. Moakes, M. Chipara, L. M. Grover, *Commun. Chem. 2021 41* **2021**, *4*, 1–8.

[30] K. Ako, *Carbohydr. Polym.* **2015**, *115*, 408–414.

[31] O. Mekmene, S. Quillard, T. Rouillon, J. M. Bouler, M. Piot, F. Gaucheron, in *Dairy*

Sci. Technol., Springer, **2009**, pp. 301–316.

[32] D. Barnum, *J. Chem. Educ.* **1999**, *76*, 938–942.

[33] L. Šimková, N. Gorodylova, Ž. Dohnalová, P. Šulcová, *Ceram. - Silikaty* **2018**, *62*, 253–260.

[34] V. Uskoković, S. Marković, L. Veselinović, S. Škapin, N. Ignjatović, D. P. Uskoković, *Phys. Chem. Chem. Phys.* **2018**, *20*, 29221–29235.

[35] S. Rollin-Martinet, A. Navrotsky, E. Champion, D. Grossin, C. Drouet, *Am. Mineral.* **2013**, *98*, 2037–2045.

[36] S. V. Dorozhkin, *J. Mater. Sci.* **2007**, *42*, 1061–1095.

[37] K. Tõnsuaadu, K. A. Gross, L. Plūduma, M. Veiderma, *J. Therm. Anal. Calorim.* **2012**, *110*, 647–659.

[38] M. P. Gashti, M. Stir, J. Hulliger, *Colloids Surfaces B Biointerfaces* **2013**, *110*, 426–433.

[39] M. . Zohuriaan, F. Shokrolahi, *Polym. Test.* **2004**, *23*, 575–579.

[40] D. Pham Minh, M. Galera Martínez, A. Nzihou, P. Sharrock, *J. Therm. Anal. Calorim.* **2013**, *112*, 1145–1155.

[41] S. Ma, L. Chen, X. Liu, D. Li, N. Ye, L. Wang, *Int. J. Green Energy* **2012**, *9*, 13–21.

[42] L. Degli Esposti, S. Markovic, N. Ignjatovic, S. Panseri, M. Montesi, A. Adamiano, M. Fosca, J. V. Rau, V. Uskoković, M. Iafisco, *J. Mater. Chem. B* **2021**, *9*, 4832–4845.

[43] R. Sun, M. Åhlén, C.-W. Tai, É. G. Bajnóczi, F. de Kleijne, N. Ferraz, I. Persson, M. Strømme, O. Cheung, *Nanomaterials* **2019**, *10*, 20.

[44] B. V. Derjaguin, V. M. Muller, Y. P. Toporov, *J. Colloid Interface Sci.* **1975**, *53*, 314–326.